

Short communication

A quantification method for peroxyacetyl nitrate (PAN) using gas chromatography (GC) with a non-radioactive pulsed discharge detector (PDD)

Lei Zhang^{a,*}, Daniel A. Jaffe^{a,b}, Xin Gao^a, Crystal D. McClure^b

^a School of Science, Technology, Engineering and Mathematics, University of Washington Bothell, Bothell, WA 98011, United States

^b Department of Atmospheric Sciences, University of Washington, Seattle, WA 98195, United States

ARTICLE INFO

Keywords:

Peroxyacetyl nitrate
Gas chromatography
Pulsed discharge detector
Non-radioactive

ABSTRACT

In this study, we developed a method for continuous PAN measurements by gas chromatography (GC) with a non-radioactive pulsed discharge detector (PDD). Operational parameters were optimized based on the ratio of peak height over baseline noise (P/N ratio). The GC/PDD system was compared with a traditional radioactive electron-capture detector (ECD). In the lab, the method detection limit (MDL) of the new GC/PDD method (9 pptv) was lower than the radioactive GC/ECD method (15 pptv), demonstrating its excellent potential. The MDL of GC/PDD in the field campaign at the Mt. Bachelor Observatory (MBO) was 23 pptv, higher than in the lab. This was caused in part by the decreased slope of the calibration curve resulting from the low air pressure level at MBO. However, the MDL level of GC/PDD at MBO is still low enough for accurate PAN measurements, although special attention should be paid to its application at high-elevation sites. Observations of PAN were conducted at MBO in the summer of 2016 with the GC/PDD system, and provided more evidence of the performance of the system. PAN was found to be highly correlated with CO. The promising performance of GC/PDD which does not require a radioactive source makes it a useful approach for accurate PAN measurements in the field.

1. Introduction

Peroxyacetyl nitrate (PAN) is a useful indicator of photochemical smog and acts as a potentially significant reservoir of nitrogen oxides (NO_x) in the troposphere (Nielsen et al., 1981; Singh and Hanst, 1981; Singh and Salas, 1983). PAN is highly stable in the cold regions of the middle and upper troposphere providing NO_x storage and hemispheric-scale transport (Singh et al., 1986), and has been recognized as a dominant form of reactive nitrogen (NO_y) in the free troposphere (Koike et al., 2003). The lifetime of PAN, due to thermal decomposition, ranges from a few hours to several months, depending on temperature (Singh, 1987). Photolysis is the main loss process of PAN in the upper troposphere (Talukdar et al., 1995). The thermal decomposition of PAN redistributes NO_x far from its source region, enhancing ozone (O₃) production in descending Asian plumes observed in the western U.S. (Heald et al., 2003; Kotchenruther et al., 2001a, b; Moxim et al., 1996; Zhang et al., 2008).

PAN decomposition was found to contribute 11%–30% toward NO_x production and enhance O₃ photochemical tendency by 0.13–0.41 ppbv d^{−1} in the springtime northeastern Pacific troposphere (Kotchenruther et al., 2001a). Ford et al. (2002) measured PAN in

ambient and snowpack interstitial air at Summit, Greenland, and found that PAN represented 30%–60% of NO_y and snowpack acted as a source of PAN in summer. PAN was found to contribute about 20% to NO_y on average at the remote Jungfraujoch research station in the Swiss Alps (Whalley et al., 2004). Fischer et al. (2011) reported the springtime PAN at the Mt. Bachelor Observatory (MBO) from 2008 to 2010 and linked the interannual variability to biomass burning, transport efficiency over the central and eastern Pacific, and transport temperature. PAN elevation in urban areas in East Asia suggested a more local impact of NO_x pollution in summer and fall (Lee et al., 2012; Xu et al., 2015; Zhang et al., 2015). The study of Ungermann et al. (2016) indicated that eddy shedding provides a rapid horizontal transport pathway of Asian pollution into the extratropical lowermost stratosphere with a timescale of only a few days. In regional wildfire plumes, ΔPAN/ΔCO ranged from 1.46–6.25 pptv ppbv^{−1} and PAN represented 25%–57% of the observed NO_y in aged plumes (Briggs et al., 2016). Therefore, PAN chemistry is a crucial part of the photochemical processes and the long-range transport of NO_x and O₃. Accurate PAN measurement is thus of great importance to improve the understanding of NO_x and O₃ formation and transformation.

The gas chromatography (GC) with electron capture detection

* Corresponding author.

E-mail address: lzhang12@uw.edu (L. Zhang).

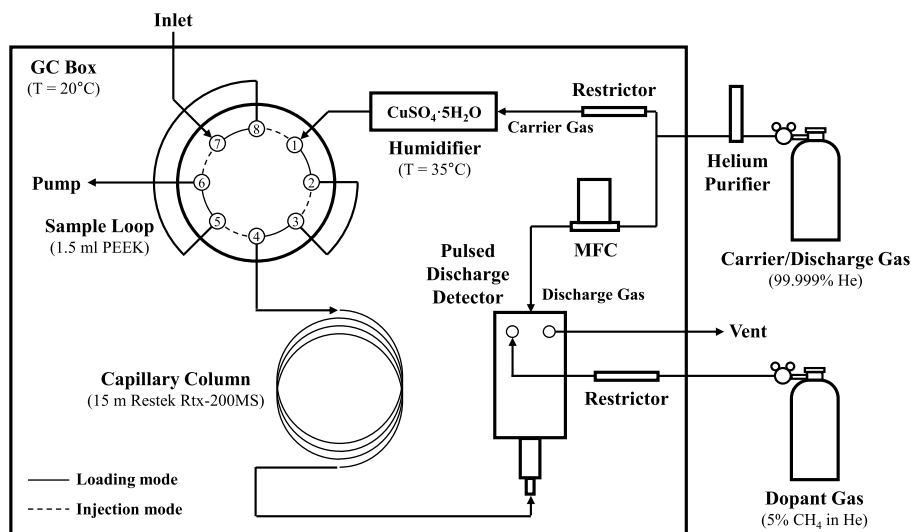


Fig. 1. Schematic diagram of the custom gas chromatograph pulsed discharge detector (GC/PDD) system.

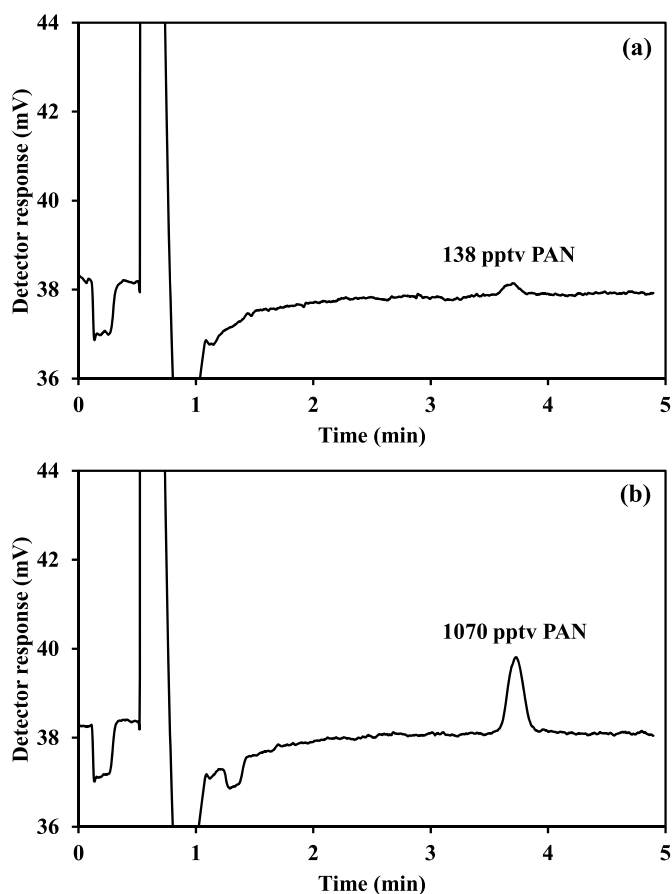


Fig. 2. Examples of PAN chromatograms: (a) response to a PAN mixing ratio of 138 pptv; (b) response to a PAN mixing ratio of 1070 pptv.

(ECD) method is hitherto the most common method to measure PAN and its homologues (Fischer et al., 2010, 2011; Flocke et al., 2005; Gao et al., 2014; Lee et al., 2013; Moravek et al., 2014; Schrimpf et al., 1995; Williams et al., 2000; Xu et al., 2015; Zellweger et al., 2000, 2003; Zhang et al., 2009; Zhang et al., 2015). Other methods have also been used, such as GC with luminol chemiluminescence detection (LCD) (Gaffney et al., 1998; Lee et al., 2012; Marley et al., 2004), GC with negative ion chemical ionization mass spectrometry (NICI-MS)

(Tanimoto et al., 1999), thermal dissociation laser-induced fluorescence (TD-LIF) (Day et al., 2002), proton-transfer-reaction mass spectrometry (PTR-MS) (Hansel and Wisthaler, 2000), and thermal dissociation chemical ionization mass spectrometry (TD-CIMS) (Slusher et al., 2004). The GC/ECD method is widely adopted for PAN measurement due to its accuracy and low method detection limit (MDL).

However, a pivotal weakness of the GC/ECD method is the radioisotope-based ECD, which uses nickel-63 (^{63}Ni) as a stable source of electrons (beta particles) that are accelerated towards a positively charged anode, generating a steady current (Fischer et al., 2010; Flocke et al., 2005; Moravek et al., 2014; Schrimpf et al., 1995; Williams et al., 2000). Because of their potentially hazardous properties, the use of radioactive materials must be closely regulated to protect the health and safety of the public and the environment. Transportation licensing and routine leak check are required for the radioactive sources, making the use of the GC/ECD method inconvenient, especially for field work. Ionization-based gas chromatographic detectors mainly include flame ionization detector (FID), thermionic ionization detector (TID), photo-ionization detector (PID), electron-capture detector (ECD), helium ionization detector (HID), and pulsed discharge detector (PDD) (Poole, 2015). PDD is actually a special type of ECD (also known as PD-ECD) using an additional dopant gas (Cai et al., 1998; Forsyth, 2004). The dopant gas is first ionized by the photons from the discharge, generating electrons which constitute the detector standing current. When electron capturing compounds enter the detector, a decrease in the detector standing current occurs, which is the PDD response. Most manufacturers will only sell a full GC, and there is no commercially available GC that would be appropriate to use for PAN. The advantage of the PDD is that it is non-radioactive and can be purchased stand-alone with a compatible electrometer without having to dismantle a GC. Ford et al. (2002) described the use of a GC/PD-ECD system to measure PAN, but provide no information on the operating characteristics or performance.

In this study we developed a GC/PDD method for PAN measurement. As an alternative to the traditional radioactive GC/ECD method, the GC/PDD combination provides high accuracy and low MDL. The GC/PDD method has enhanced deployability due to its non-radioactive source. We compared the two methods in the lab using a state-of-the-art calibration system, and employed the GC/PDD method in the 2016 summer campaign at the Mt. Bachelor Observatory (MBO, 2.8 km asl) to evaluate its on-site performance. Overall the GC/PDD method has similar or better performance as the radioactive GC/ECD method.

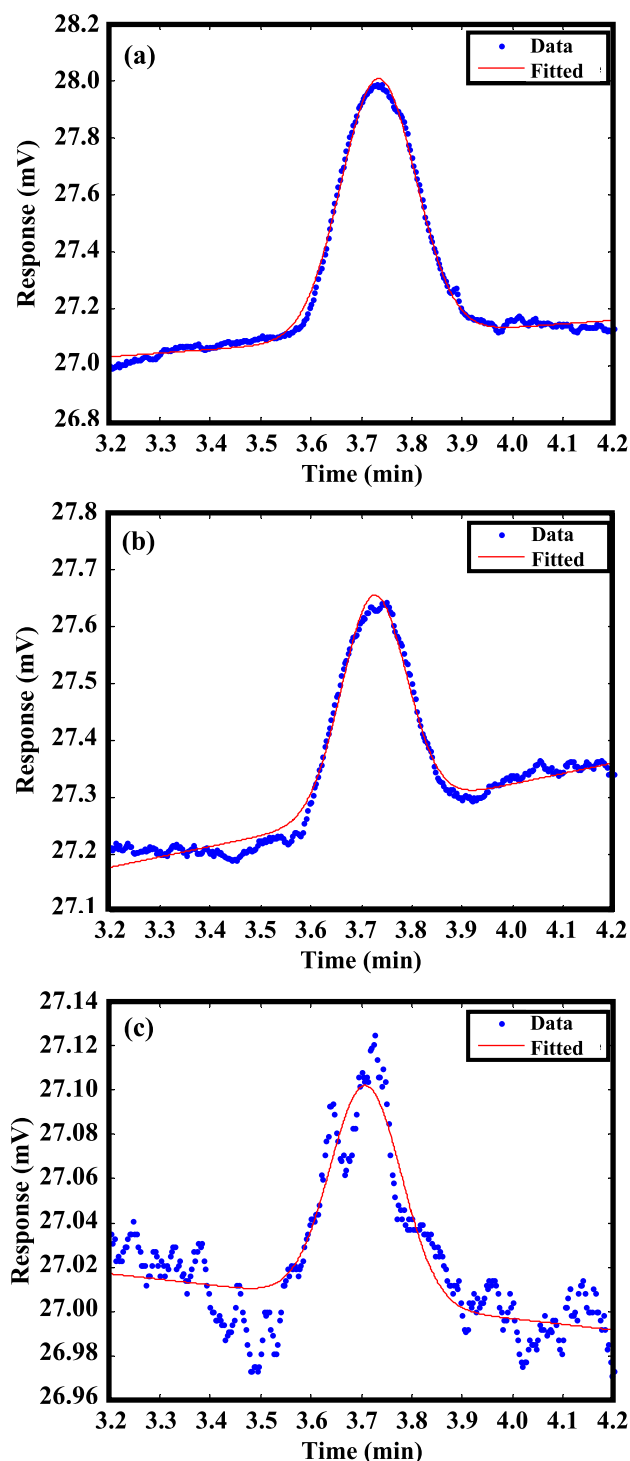


Fig. 3. Examples of PAN chromatogram fittings using MATLAB: (a) response to a PAN mixing ratio of 1070 pptv; (b) response to a PAN mixing ratio of 438 pptv; (c) response to a PAN mixing ratio of 138 pptv.

2. Materials and methods

The GC/PDD PAN detection system consisted of a capillary GC column, a Valco Instruments Co. Inc. (VICI) PDD Model D-2, an 8-port valve with a sample loop, a pump, a humidifier, a helium gas cylinder with a helium purifier, a dopant gas cylinder, a mass flow controller (MFC), and two restrictors (Fig. 1). Similar to the system described by Fischer et al. (2010), the system incorporated a photochemical PAN

calibration source using a calibrated nitric oxide (NO) standard and excess acetone to generate PAN under illumination of an ultraviolet (UV) lamp (Fischer et al., 2010).

2.1. PAN detection system

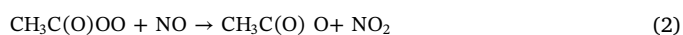
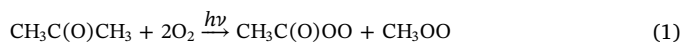
An 8-port Valco valve was utilized to control the operational modes of the system. Under the loading mode, air samples were collected through the inlet to a 1.5 mL sample loop by a pump. The sample loop is made from 1/8" polyetheretherketone (PEEK) tubing. PEEK tubing was reported to have no loss of PAN and a better performance than perfluoroalkoxy (PFA) and stainless steel tubing (Fischer et al., 2010; Flocke et al., 2005). Oxygen (O_2) diffuses through PFA tubing, causing a noisy background, and PAN loss has been observed on stainless steel. Ultra-high purity (UHP) helium (He) was used as a carrier/discharge gas. UHP He was further purified with an Agilent Gas Clean Filter System to remove O_2 and moisture. The carrier gas flow rate was set to be 7 mL min^{-1} using a Valco restrictor. Prior to entering the valve and column the carrier gas was humidified by a cartridge filled with 200 g of copper sulfate pentahydrate ($CuSO_4 \cdot 5H_2O$, 99.995% purity), temperature controlled to 35°C (Flocke et al., 2005). The addition of moisture minimizes loss of PAN in the column, valve and tubing. The filling in the cartridge was changed every two months.

When the 8-port valve switches to the injection mode, the purified and humidified carrier gas passes through the valve and a 1/16" PEEK connecting tubing, and enters the column. We used a 15 m Restek Rtx-200MS (1 mm film thickness, 0.53 mm inner diameter) capillary column. The column was controlled to 20°C by a bidirectional temperature controller (TE Technology TC 36-25 RS232) and a thermoelectric device (TE Technology AC-073). The sample flow enters one end of the VICI PDD which was controlled to 60°C for detection. The PDD used 30 mL min^{-1} UHP He as a discharge gas and 1.8 mL min^{-1} of 5% methane (CH_4) in He as a dopant gas. The flow rates of the discharge gas and the dopant gas were controlled with an MFC and a Valco restrictor, respectively.

The PDD was set to the electron capture mode which requires the addition of a dopant gas. The dopant gas used in this study is first ionized by the photons from the discharge gas generating electrons. When compounds that can capture electrons enter the detector the standing current in the PDD is decreased. Before tests the detector was baked at 300°C for 12 h to stabilize its background. The output voltage signal from the detector was converted to a digital signal by the PeakSimple Chromatography Data System, and the PeakSimple software was used to collect the output from the detector. With the above mentioned conditions, the PAN peak occurs at about 3.6 min (within the range of 3.3–3.9 min). Samples were collected every 5 min.

2.2. PAN calibration source

The PAN calibration source was also used in our previous study (Fischer et al., 2010). We used NO and excess acetone in the presence of O_2 and UV to generate PAN. NO is converted to NO_2 and then to PAN following Reactions (1) to (4) (Fischer et al., 2010; Roberts et al., 2004):



The conversion efficiency of the calibrator from NO to PAN is $93 \pm 3\%$ based on previous work (Fischer et al., 2010; Flocke et al., 2005). We used Scott-Marrin standard cylinders with a NO mixing ratio of 0.996 ppmv and an acetone mixing ratio of 20 ppmv in ultrapure air.

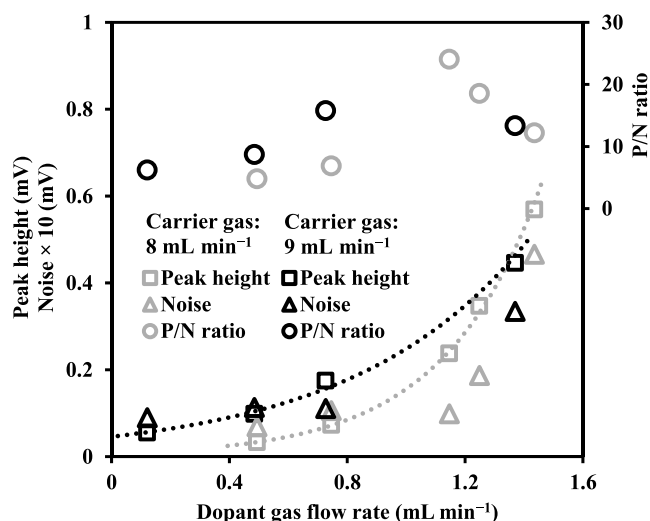


Fig. 4. Peak heights, baseline noises and the ratios between them (P/N ratio) under different carrier gas and dopant gas flow rates. Baseline noise is represented by the standard deviation of the baseline within a 1-min range in the vicinity of the peak.

Table 1

Calibration parameters, method detection limits (MDLs) and overall uncertainties of GC/PDD and GC/ECD at UWB and MBO.

Parameters	GC/PDD		GC/ECD	
	UWB	MBO	UWB	MBO
Slope for calibration (mV s pptv^{-1})	10.0	4.1	65.9	45.2
R^2 for calibration	0.997	0.996	0.997	0.994
MDL (pptv)	9	23	15	15 ^a
Uncertainty at ~ 1000 pptv (%)	8.1	9.8	7.7	8.2 ^a

Note: ^a These estimations were adapted from Fischer et al. (2010).

Both gas cylinders were National Institute of Standards and Technology (NIST)-traceable ($\pm 2\%$ tolerance). The flow rates of NO and acetone were 1.2 and 38 mL min^{-1} , respectively, controlled by MFCs. PAN from the calibrator was diluted with hydrocarbon free (HCF) air from a pressurized cylinder. The flow rate of HCF air ranged from 660 to 5000 mL min^{-1} to generate a range of PAN mixing ratios from 221 to 1590 pptv. The system requires approximately 30 min to produce a steady PAN calibration source.

2.3. Comparison with a GC/ECD system

To evaluate the performance of the GC/PDD system, we compared it to the GC/ECD system used in our previous study (Fischer et al., 2010). The same GC with the same configuration was used, but the PDD was replaced with a Shimadzu Mini-2 ECD. The temperature of the ECD was controlled to 40 °C. UHP He was used as a carrier gas at a flow rate of 27–28 mL min^{-1} , and UHP nitrogen (N_2) was used as a make-up gas at a flow rate of 2–3 mL min^{-1} . Uncertainties, sensitivities, and MDLs of these two methods were compared using the same PAN calibration source. Three sets of calibrations using the GC/PDD method were conducted to ensure its stability. Either two sets were at least one week away from each other, including a 6-point calibration each time.

2.4. Application in the 2016 summer campaign at MBO

The GC/PDD method was deployed in the 2016 summer campaign at the Mt. Bachelor Observatory (MBO). MBO is located on the summit of a dormant volcano in central Oregon (43°58'39" N 121°41'10" W, 2763 m asl). The site has been used for atmospheric chemistry research for over 13 years (Jaffe et al., 2005). The PAN measurement in the

campaign took place from July 29 to September 27, 2016. The campaign lasted for two months and two sets of calibrations were performed within the campaign. Sub-micron aerosol scattering coefficient (σ_{sp}) and carbon monoxide (CO) were also measured during the campaign. We used a multi-wavelength nephelometer Model 3563 manufactured by TSI Inc. to measure sub-micron aerosol scattering at 450, 550 and 700 nm (blue, green and red) (Laing et al., 2016). The σ_{sp} at green wavelength are adjusted to standard temperature and pressure condition (STP, 273 K and 1 atm) for analysis in this study. CO was measured using a Picarro G2302 cavity ring-down spectrometer (Gratz et al., 2015). All data are reported every 5 min in the Coordinated Universal Time (UTC).

2.5. Backward trajectories and wildfire locations

We calculated 10-day air mass backward trajectories from MBO for every hour of the two identified plume events using the Hybrid Single-Particle Lagrangian Integrated Trajectory (HYSPPLIT) model version 4 (Draxler and Hess, 1998). Global Data Assimilation System (GDAS) $1^\circ \times 1^\circ$ gridded meteorological data were used. The starting height was set to be 1800 m above ground level based on terrain height in the gridded meteorological data (Gratz et al., 2015). Daily MODIS fire detection data for North America was obtained from the United States Department of Agriculture (USDA) Forest Service (<http://activefiremaps.fs.fed.us/gisdata.php>). Daily MODIS fire detection data for Eurasia was downloaded from the Fire Information for Resource Management System (FIRMS) of the US National Aeronautics and Space Administration (NASA) (<https://firms.modaps.eosdis.nasa.gov/download>).

3. Results and discussion

3.1. Chromatogram integration and operational parameters

Fig. 2 shows the chromatograms of two samples from the calibration source with PAN mixing ratios of 138 and 1070 pptv. The PAN signals occurred at about 3.7 min. The chromatograms from the GC/PDD method indicate good performance and low MDL of the system. We developed an integration method for the chromatogram using MATLAB. Peak fitting was performed within a 1-min range in the vicinity of the peak using a Modified Gaussian Equation (MGE):

$$f(x) = \lambda_1 \exp \left[-\left(\frac{x - \lambda_2}{\lambda_3} \right)^2 \right] + \lambda_4 + \lambda_5 x \quad (5)$$

In Equation (5), λ_1 is a scale factor of the peak; λ_2 is the center of the peak; λ_3 is a width factor of the peak; λ_4 is the baseline offset; and λ_5 is the baseline slope. We then integrated the fitted line to obtain the peak area for the PAN signal. Fig. 3 shows the chromatograms and their fitted lines of three samples from the PAN source in a calibration case with a fluctuating baseline. The MGE method exhibits an excellent fit for both high and low signal cases (Fig. 3).

The flow rates of carrier gas and dopant gas are crucial operational parameters affecting the performance of the GC/PDD system. Baseline noise is represented by the standard deviation of the baseline within a 1-min range in the vicinity of the peak. The ratio of peak height over baseline noise (P/N ratio) is an important indicator to depict the performance of the system. Therefore, we fixed the PAN mixing ratio to 862 pptv, and changed the flow rates of carrier gas and dopant gas. Peak heights, baseline noises and the P/N ratios under different conditions are shown in Fig. 4. Peak height and baseline noise both increase when the dopant gas flow rate increases, while the P/N ratio climbs up first and then declines. High P/N ratio implies high detectability. Therefore, there is an optimal dopant gas flow rate. Two sets of tests were conducted when carrier gas flow rates were set to be 8 and 9 mL min^{-1} , respectively. Under high dopant gas condition

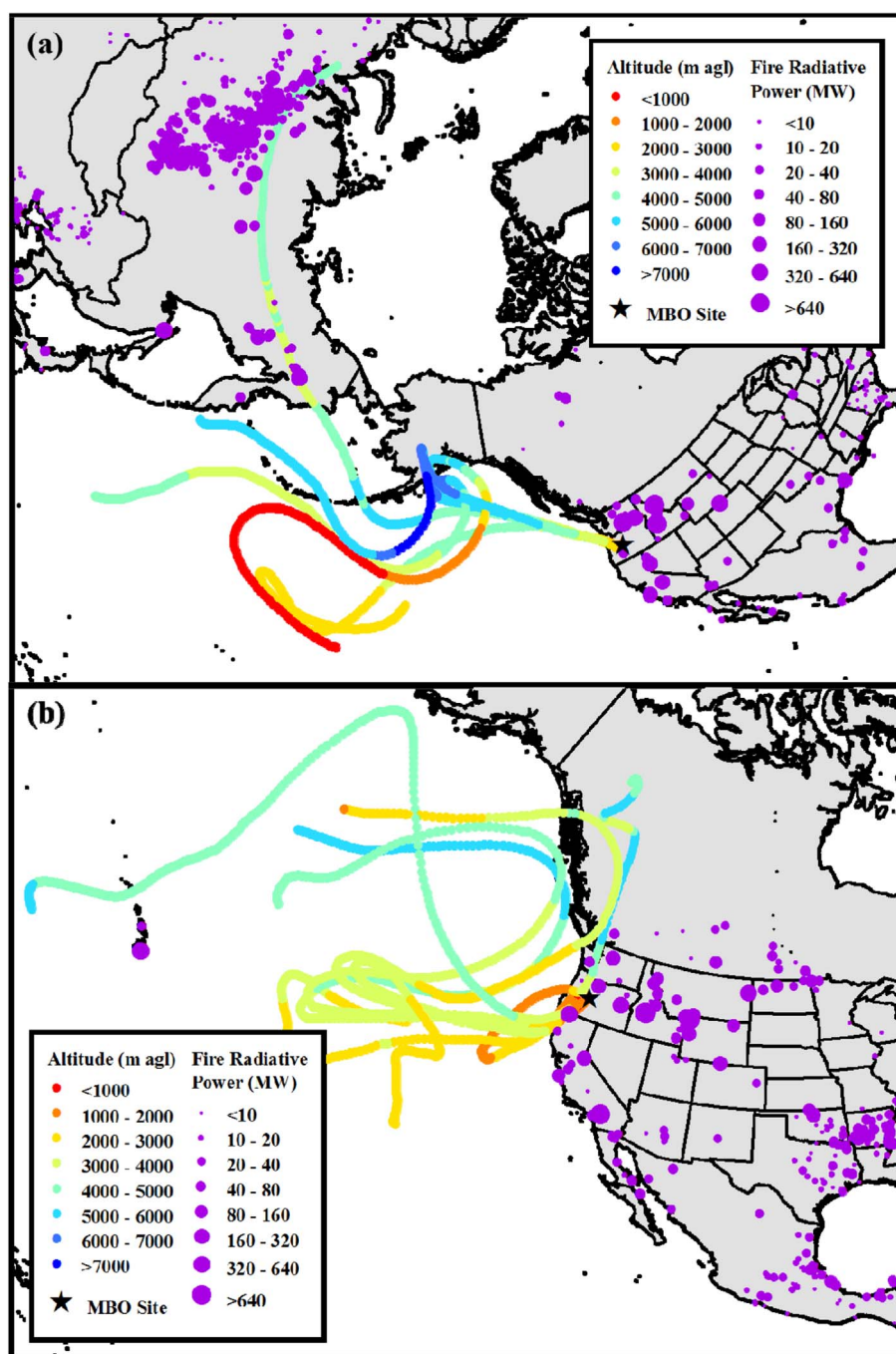


Fig. 5. Backward trajectories for (a) Event 1 (2016/7/31 6:00–2016/8/1 5:00) with Asian fire locations on July 24, 2016 and North American fire locations on July 31, 2016, and (b) Event 2 (2016/8/30 8:00–2016/9/1 4:00) with North American fire locations on August 30–31, 2016.

(> 1.5 mL min^{−1}), reducing the carrier gas also has an increasing effect for both peak height and baseline noise, and there is also an optimal carrier gas flow rate. The tests showed in Fig. 4 were taken place in the lab (1 013 hPa and 293 K). For MBO (730 hPa and 293 K), the optimal operational parameters were a bit different from the lab due to the air pressure discrepancy. At MBO, slightly lower carrier gas flow rate (7 mL min^{−1}) and slightly higher dopant gas flow rate (1.8 mL min^{−1}) were used, although we did not do the same extensive set of test conditions as in the lab.

3.2. Comparisons between GC/ECD and GC/PDD

Comparisons between GC/ECD and GC/PDD were conducted both

in the lab at the University of Washington Bothell (UWB) and at MBO. The same calibration source was used for the two detection systems at 6–7 PAN mixing ratio levels. Parameters for calibrations are shown in Table 1. The calibrations by GC/ECD and GC/PDD at UWB, have high correlations ($R^2 = 0.997$) and show good linearity. The most important parameter to evaluate the performance of the two methods is the method detection limit (MDL), which is defined as three times the standard deviation of the replicates of a low calibration standard over the slope of the calibration curve. It is often used when the noise for the blank is not available, which is true in chromatography. MDLs were calculated using the following equation:

$$\text{MDL} = \frac{3\sigma}{s} \quad (6)$$

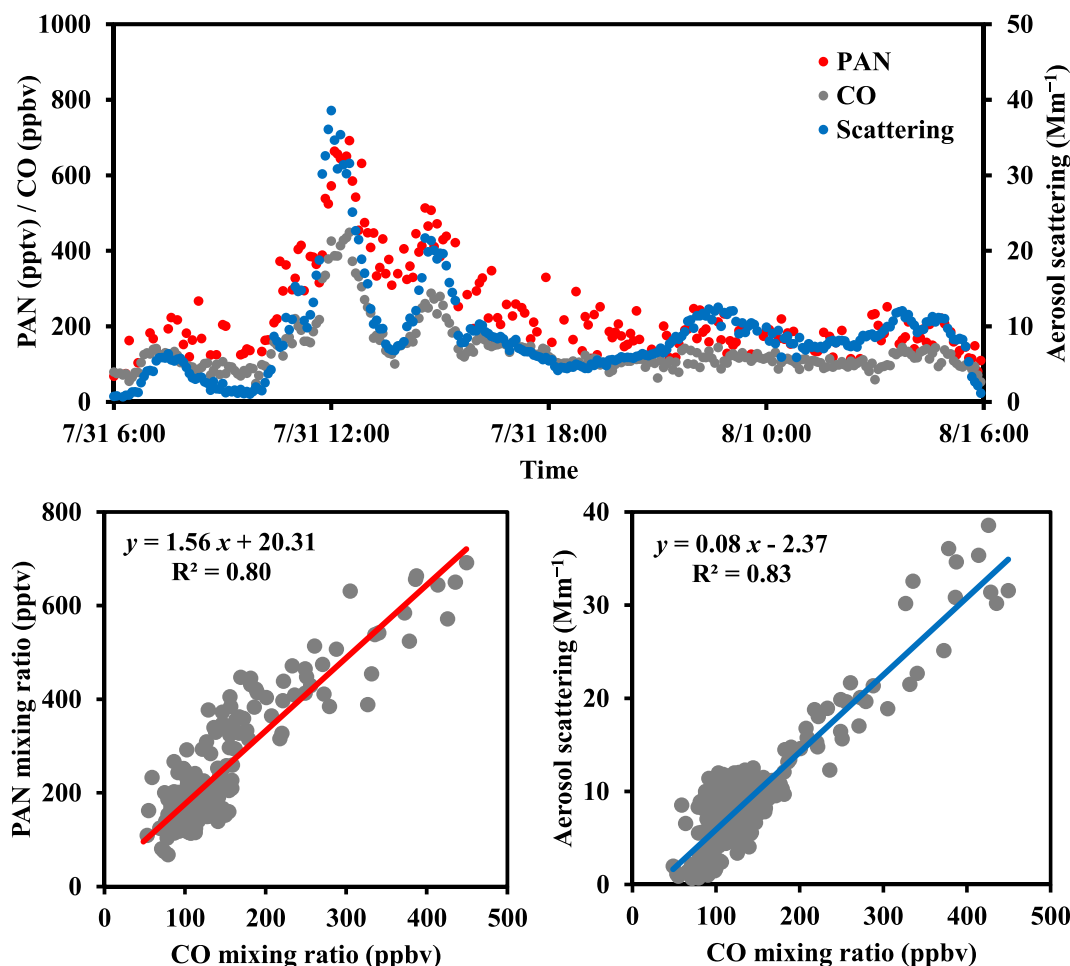


Fig. 6. Observations of PAN, CO and aerosol scattering coefficient at MBO during Event 1 from July 31 to August 1, 2016, a period with significant influence from Siberian wildfire smokes. The scatter plots show the data fit with linear regression.

In Equation (6), s is the slope of the calibration curve (mV s pptv^{-1}), and σ is the standard deviation of the peak area (mV s) at the lowest PAN mixing ratio (~ 200 pptv) during calibration. The standard deviations for GC/ECD and GC/PDD at ~ 200 pptv in the lab were 0.34 and 0.031 mV s, respectively. Therefore, with the obtained slopes, the corresponding MDLs were 15 and 9 pptv, respectively. The precisions of the two systems at ~ 1000 pptv were estimated to be 0.4% and 2.5% from replicate observations. The accuracy of the PAN mixing ratio produced by the calibrator was estimated to be 7.7% by our previous study (Fischer et al., 2010). The overall uncertainty was calculated as the root sum of the squares of the precision and the accuracy. Therefore, the overall uncertainties for GC/ECD and GC/PDD at UWB were found to be 7.7% and 8.1% (at ~ 1000 pptv), respectively (see Table 1).

With the same method, the precision of the system at MBO at ~ 1000 pptv was estimated to be 6.1%. With the precision (6.1%) and the accuracy (7.7%), the overall uncertainty of the GC/PDD method at MBO was reported to be 9.8% at ~ 1000 pptv (see Table 1), compared to 8.2% using GC/ECD method at MBO (Fischer et al., 2010). In the calibration at MBO during the 2016 summer campaign, the standard deviation was 0.031 mV s. Therefore, with Equation (6), the MDL for the campaign was estimated to be 23 pptv (see Table 1), higher than the MDL at UWB (9 pptv). This was caused by the decreased slope of the calibration curve ($4.1 \text{ mV s pptv}^{-1}$) resulting from the low air pressure level (~ 730 mbar) at MBO, compared to the slope at UWB ($10.0 \text{ mV s pptv}^{-1}$). The slopes were lower at MBO for both methods. This was due to the lower air pressure at the high elevation MBO site. The air pressure difference between UWB and MBO causes the change of the total sample volume resulting in a $\sim 30\%$ loss in the injection mass.

Furthermore, the pressure discrepancy has a more significant impact on the slope for GC/PDD than that for GC/ECD. The larger sensitivity reduction suggests that the PDD detector also has a pressure dependence, but we don't have any further evidence on how it works. However, the MDL level of GC/PDD at MBO is still low enough for accurate PAN measurements, although special attention should be paid to its application at high-elevation sites.

3.3. Plume events in the 2016 summer campaign at MBO

Measurements of PAN were made at MBO from July 29 to September 27, 2016. Totally 7622 valid PAN data (5-min) were obtained from the 2016 summer campaign at MBO. The mean PAN mixing ratio was 221 pptv, and the median value was 194 pptv. The 5th–95th percentile range was 87–434 pptv. Observations of PAN at MBO in summer 2016 fit a lognormal distribution, reflecting the background PAN level in the western U.S. and influence from regional and long-range transport wildfires. To evaluate the performance of the GC/PDD method in pollution episodes, we chose two typical plume events in the 2016 summer campaign at MBO for multi-pollutant analysis. Fig. 5 shows the 10-day backward trajectories for the two plume events with wildfire locations in North America during the events and in Eurasia one week before the events which is the approximate transport time of air masses. Event 1 was under significant influence of Siberian wildfires, especially at lower elevation in eastern Russia, and the backward trajectories of Event 1 had no overlap with regional wildfires in North America. On the contrary, Event 2 was transported from large fires in northern California.

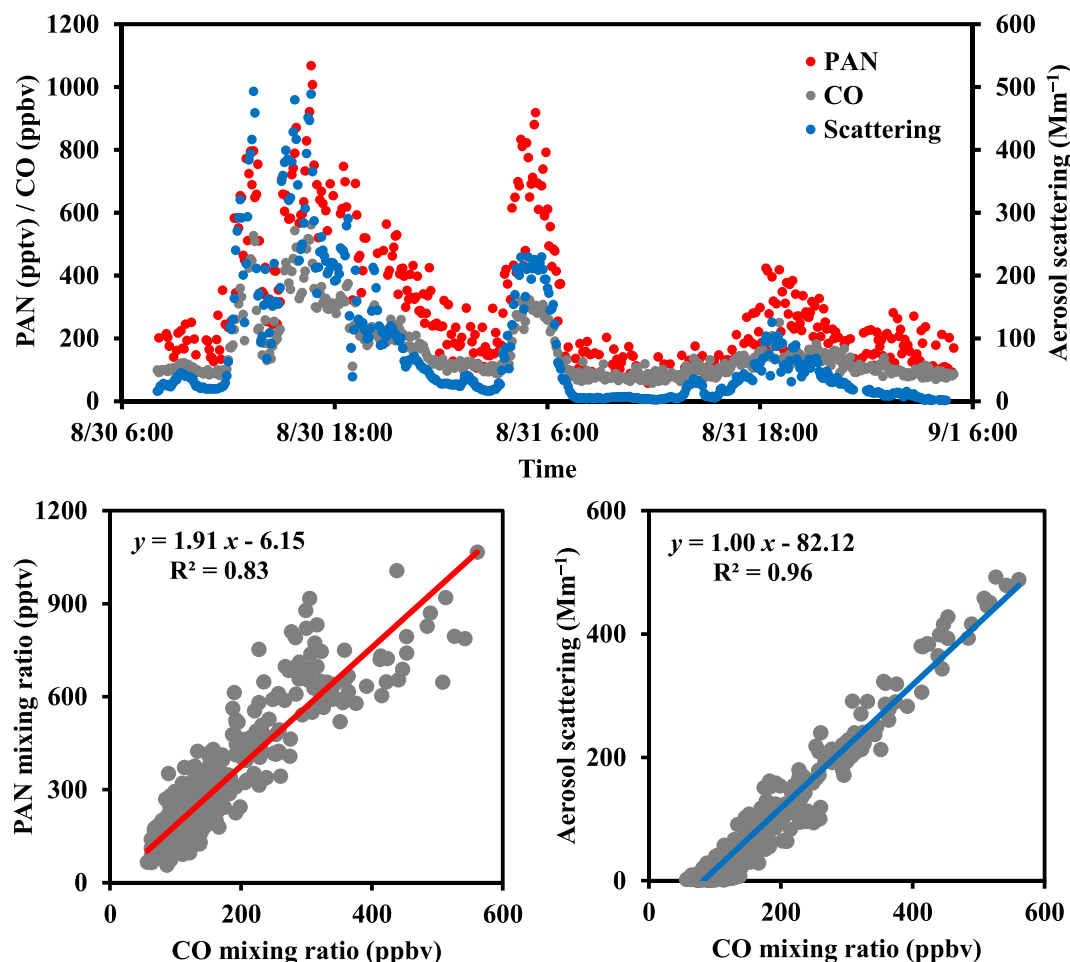


Fig. 7. Observations of PAN, CO and aerosol scattering coefficient at MBO during Event 2 from August 30 to September 1, 2016, a period with significant influence from regional (northern California) wildfire smokes. The scatter plots show the data fit with linear regression.

Fig. 6 and Fig. 7 exhibit the observations of PAN, CO and aerosol scattering (σ_{sp}) during Event 1 and Event 2, respectively. Event 1 experienced two peaks at 12:00 and 15:00 UTC on July 31, and Event 2 had a longer pollution episode from 12:00–19:00 on August 30 and two separate peaks at 5:00 and 19:00 on August 31. CO and PAN had significant positive correlations in both events ($R^2 > 0.8$). The correlation between CO and σ_{sp} was even more significant, especially for Event 2 ($R^2 = 0.96$). The enhancement ratios (ERs) of $\Delta\text{PAN}/\Delta\text{CO}$ for Event 1 and Event 2 were 1.56 and 1.91 pptv ppbv⁻¹, respectively, close to the lower end of the range (1.46–6.25 pptv ppbv⁻¹) reported by Briggs et al. (2016) for regional wildfire plumes. Much more significant difference occurred on the ERs of $\Delta\sigma_{sp}/\Delta\text{CO}$ for Event 1 (0.08 Mm⁻¹ ppbv⁻¹) and Event 2 (1.00 Mm⁻¹ ppbv⁻¹). The comparison between the Siberian wildfire event (Event 1) and the regional wildfire event (Event 2) indicates that aerosols generated from wildfires could be scavenged during long-range transport (Zhang and Jaffe, 2017) while PAN is not significantly scavenged by cloud processing. The PAN level in wildfire plumes is more likely related to the air temperature. In 2 Siberian wildfire plume events in spring 2008 (Fischer et al., 2010), the $\Delta\text{PAN}/\Delta\text{CO}$ ratios were 4.0 and 6.3 pptv ppbv⁻¹ under an average air temperature of -3°C observed at MBO, much higher than in the 2 wildfire plume events identified in the 2016 summer campaign at an average air temperature of 11°C at MBO. This could be resulted from the shift of NO_x –PAN balance towards the PAN side at lower temperature (Singh and Hanst, 1981). However, temperature is not the only factor. Fire emission ratios of NO_x/CO and photochemical conditions are also very important to PAN formation (Fischer et al., 2014). The high correlation between CO and PAN in

different types of plume events and the relationship between temperature and $\Delta\text{PAN}/\Delta\text{CO}$ provided more evidence on the reliability of the new GC/PDD method.

4. Conclusion

We developed a new method for PAN measurements using GC with a non-radioactive PDD. The system was optimized and calibrated using PAN generated from a calibrated source of NO and excess acetone in the presence of O₂ and UV. A Modified Gaussian Equation (MGE) method was used for peak fitting to smooth the signal at low PAN mixing ratio levels considering a sloping baseline. The new GC/PDD method was compared to the traditional GC/ECD method in the lab. The MDL of GC/PDD operated in the lab was 9 pptv, lower than that of GC/ECD (15 pptv), showing the excellent performance of the GC/PDD system. The MDL of GC/PDD at MBO was 23 pptv while the MDL of GC/ECD at MBO stayed the same (15 pptv). The sensitivity reduction for GC/PDD was due to the lower air pressure at the high elevation MBO site. Besides the sample volume loss, the PDD detector also has a pressure dependence. However, the MDL level at MBO is still low enough for accurate PAN measurements. The overall uncertainties for GC/ECD and GC/PDD in the lab at ~ 1000 pptv were 7.7% and 8.1%, respectively, while that for GC/PDD at MBO was found to be 9.8%. The new method was used in the 2016 summer campaign at MBO. Based on the analyses of wildfire plume events, PAN was found to be highly correlated with CO. Results of enhancement ratios show that aerosols could be largely scavenged during long-range transport while the PAN level is more likely related to the air temperature. The similar levels of significance for the CO–PAN

correlations between GC/ECD and GC/PDD and the similar Δ PAN/ Δ CO ratios obtained from these two methods for the same types of events provided more evidence on the reliability of the GC/PDD method. Results in this study indicate that the performance of the new GC/PDD method is almost as good as GC/ECD. With its non-radioactive essence, GC/PDD could be widely applied to continuous PAN measurements in the ambient air.

Acknowledgment

This study was funded by the National Science Foundation (grant #AGS-1447832) and the National Oceanic and Atmospheric Administration (contract #RA-133R-16-SE-0758). HYSPLIT data were processed by Jonathan Hee. Editing assistance was provided by Dee Ann Lommers-Johnson. MBO data are permanently archived at the University of Washington data repository (<https://digital.lib.washington.edu/researchworks>).

References

- Briggs, N.L., Jaffe, D.A., Gao, H., Hee, J.R., Baylon, P.M., Zhang, Q., Zhou, S., Collier, S.C., Sampson, P.D., Cary, R.A., 2016. Particulate matter, ozone, and nitrogen species in aged wildfire plumes observed at the Mount Bachelor Observatory. *Aerosol Air Qual. Res.* 16, 3075–3087.
- Cai, H., Stearns, S.D., Wentworth, W.E., 1998. Pulsed discharge electron capture detector operating in the constant-current mode by means of feedback dc bias voltage. *Anal. Chem.* 70, 3770–3776.
- Day, D.A., Wooldridge, P.J., Dillon, M.B., Thornton, J.A., Cohen, R.C., 2002. A thermal dissociation laser-induced fluorescence instrument for in situ detection of NO₂, peroxy nitrates, alkyl nitrates, and HNO₃. *J. Geophys. Res.* 107, 4046.
- Draxler, R.R., Hess, G.D., 1998. An overview of the HYSPLIT 4 modelling system for trajectories, dispersion and deposition. *Aust. Meteorol. Mag.* 47, 295–308.
- Fischer, E.V., Jaffe, D.A., Reidmiller, D.R., Jaeglé, L., 2010. Meteorological controls on observed peroxyacetyl nitrate at Mount Bachelor during the spring of 2008. *J. Geophys. Res.* 115, D03302.
- Fischer, E.V., Jaffe, D.A., Weatherhead, E.C., 2011. Free tropospheric peroxyacetyl nitrate (PAN) and ozone at Mount Bachelor: potential causes of variability and timescale for trend detection. *Atmos. Chem. Phys.* 11, 5641–5654.
- Fischer, E.V., Jacob, D.J., Yantosca, R.M., Sulprizio, M.P., Millet, D.B., Mao, J., Paulot, F., Singh, H.B., Roiger, A., Ries, L., Talbot, R.W., Dzepina, K., Pandey Deolal, S., 2014. Atmospheric peroxyacetyl nitrate (PAN): a global budget and source attribution. *Atmos. Chem. Phys.* 14, 2679–2698.
- Flocke, F.M., Weinheimer, A.J., Swanson, A.L., Roberts, J.M., Schmitt, R., Shertz, S., 2005. On the measurement of PANs by gas chromatography and electron capture detection. *J. Atmos. Chem.* 52, 19–43.
- Ford, K.M., Campbell, B.M., Shepson, P.B., Bertman, S.B., Honrath, R.E., Peterson, M., Dibb, J.E., 2002. Studies of Peroxyacetyl nitrate (PAN) and its interaction with the snowpack at Summit, Greenland. *J. Geophys. Res.* 107, 4102.
- Forsyth, D.S., 2004. Pulsed discharge detector: theory and applications. *J. Chromatogr. A* 1050, 63–68.
- Gaffney, J.S., Bornick, R.M., Chen, Y.H., Marley, N.A., 1998. Capillary gas chromatographic analysis of nitrogen dioxide and PANs with luminol chemiluminescent detection. *Atmos. Environ.* 32, 1445–1454.
- Gao, T., Han, L., Wang, B., Yang, G., Xu, Z., Zeng, L., Zhang, J., 2014. Peroxyacetyl nitrate observed in Beijing in August from 2005 to 2009. *J. Environ. Sci.* 26, 2007–2017.
- Gratz, L.E., Jaffe, D.A., Hee, J.R., 2015. Causes of increasing ozone and decreasing carbon monoxide in springtime at the Mt. Bachelor Observatory from 2004 to 2013. *Atmos. Environ.* 109, 323–330.
- Hansel, A., Wisthaler, A., 2000. A method for real-time detection of PAN, PPN and MPAN in ambient air. *Geophys. Res. Lett.* 27, 895–898.
- Heald, C.L., Jacob, D.J., Fiore, A.M., Emmons, L.K., Gille, J.C., Deeter, M.N., Warner, J., Edwards, D.P., Crawford, J.H., Hamlin, A.J., Sachse, G.W., Browell, E.V., Avery, M.A., Vay, S.A., Westberg, D.J., Blake, D.R., Singh, H.B., Sandholm, S.T., Talbot, R.W., Fuelberg, H.E., 2003. Asian outflow and trans-Pacific transport of carbon monoxide and ozone pollution: an integrated satellite, aircraft, and model perspective. *J. Geophys. Res.* 108, 4804.
- Jaffe, D., Prestbo, E., Swartzendruber, P., Weisspenzias, P., Kato, S., Takami, A., Hatakeyama, S., Kajii, Y., 2005. Export of atmospheric mercury from Asia. *Atmos. Environ.* 39, 3029–3038.
- Koike, M., Kondo, Y., Kita, K., Takegawa, N., Masui, Y., Miyazaki, Y., Ko, M.W., Weinheimer, A.J., Flocke, F., Weber, R.J., Thornton, D.C., Sachse, G.W., Vay, S.A., Blake, D.R., Streets, D.G., Eisele, F.L., Sandholm, S.T., Singh, H.B., Talbot, R.W., 2003. Export of anthropogenic reactive nitrogen and sulfur compounds from the East Asia region in spring. *J. Geophys. Res.* 108, 8789.
- Kotchenruther, R.A., Jaffe, D.A., Jaeglé, L., 2001a. Ozone photochemistry and the role of peroxyacetyl nitrate in the springtime northeastern Pacific troposphere: results from the photochemical ozone budget of the eastern North Pacific atmosphere (PHOBEA) campaign. *J. Geophys. Res.* 106, 28731–28742.
- Kotchenruther, R.A., Jaffe, D.A., Beine, H.J., Anderson, T.L., Bottenheim, J.W., Harris, R.W., Blake, D.R., Schmitt, R., 2001b. Observations of ozone and related species in the northeast Pacific during the PHOBEA campaigns: 2. Airborne observations. *J. Geophys. Res.* 106, 7463–7483.
- Laing, J.R., Jaffe, D.A., Hee, J.R., 2016. Physical and optical properties of aged biomass burning aerosol from wildfires in Siberia and the Western USA at the Mt. Bachelor Observatory. *Atmos. Chem. Phys.* 16, 15185–15197.
- Lee, G., Choi, H.-S., Lee, T., Choi, J., Park, J.S., Ahn, J.Y., 2012. Variations of regional background peroxyacetyl nitrate in marine boundary layer over Baengyeong Island, South Korea. *Atmos. Environ.* 61, 533–541.
- Lee, J.B., Yoon, J.S., Jung, K., Eom, S.W., Chae, Y.Z., Cho, S.J., Kim, S.D., Sohn, J.R., Kim, K.H., 2013. Peroxyacetyl nitrate (PAN) in the urban atmosphere. *Chemosphere* 93, 1796–1803.
- Marley, N.A., Gaffney, J.S., White, R.V., Rodriguez-Cuadra, L., Herndon, S.E., Dunlea, E., Volkamer, R.M., Molina, L.T., Molina, M.J., 2004. Fast gas chromatography with luminol chemiluminescence detection for the simultaneous determination of nitrogen dioxide and peroxyacetyl nitrate in the atmosphere. *RSI* 75, 4595–4605.
- Moravek, A., Foken, T., Trebs, I., 2014. Application of a GC-ECD for measurements of biosphere-atmosphere exchange fluxes of peroxyacetyl nitrate using the relaxed eddy accumulation and gradient method. *Atmos. Meas. Tech.* 7, 2097–2119.
- Moxim, W.J., Levy, H., Kasibhatla, P.S., 1996. Simulated global tropospheric PAN: its transport and impact on NO_x. *J. Geophys. Res. Atmos.* 101, 12621–12638.
- Nielsen, T., Samuelsson, U., Grennfelt, P., Thomsen, E.L., 1981. Peroxyacetyl nitrate in long-range transported polluted air. *Nature* 293, 553–555.
- Poole, C.F., 2015. Ionization-based detectors for gas chromatography. *J. Chromatogr. A* 1421, 137–153.
- Roberts, J.M., Flocke, F., Chen, G., de Gouw, J., Holloway, J.S., Hübler, G., Neuman, J.A., Nicks, D.K., Nowak, J.B., Parrish, D.D., Ryerson, T.B., Sueper, D.T., Warneke, C., Fehsenfeld, F.C., 2004. Measurement of peroxyacetic nitric anhydrides (PANs) during the ITCT 2K2 aircraft intensive experiment. *J. Geophys. Res.* 109, D23S21.
- Schrimpf, W., Müller, K.P., Johnen, F.J., Lienaerts, K., Rudolph, J., 1995. An optimized method for airborne peroxyacetyl nitrate (PAN) measurements. *J. Atmos. Chem.* 22, 303–317.
- Singh, H.B., Hanst, P.L., 1981. Peroxyacetyl nitrate (PAN) in the unpolluted atmosphere – an important reservoir for nitrogen oxides. *Geophys. Res. Lett.* 8, 941–944.
- Singh, H.B., Salas, L.J., 1983. Peroxyacetyl nitrate in the free troposphere. *Nature* 302, 326–328.
- Singh, H.B., Salas, L.J., Viezee, W., 1986. Global distribution of peroxyacetyl nitrate. *Nature* 321, 588–591.
- Singh, H.B., 1987. Reactive nitrogen in the troposphere. *Environ. Sci. Technol.* 21, 320–327.
- Slusher, D.L., Huey, L.G., Tanner, D.J., Flocke, F.M., Roberts, J.M., 2004. A thermal dissociation-chemical ionization mass spectrometry (TD-CIMS) technique for the simultaneous measurement of peroxyacetyl nitrates and dinitrogen pentoxide. *J. Geophys. Res.* 109, D19315.
- Talukdar, R.K., Burkholder, J.B., Schmoltner, A.M., Roberts, J.M., Wilson, R.R., Ravishankara, A.R., 1995. Investigation of the loss processes for peroxyacetyl nitrate in the atmosphere: UV photolysis and reaction with OH. *J. Geophys. Res.* 100, 14163–14173.
- Tanimoto, H., Hirokawa, J., Kajii, Y., Akimoto, H., 1999. A new measurement technique of peroxyacetyl nitrate at parts per trillion by volume levels: gas chromatography/negative ion chemical ionization mass spectrometry. *J. Geophys. Res.* 104, 21343–21354.
- Ungermann, J., Ern, M., Kaufmann, M., Müller, R., Spang, R., Ploeger, F., Vogel, B., Riese, M., 2016. Observations of PAN and its confinement in the Asian summer monsoon anticyclone in high spatial resolution. *Atmos. Chem. Phys.* 16, 8389–8403.
- Whalley, L.K., Lewis, A.C., McQuaid, J.B., Purvis, R.M., Lee, J.D., Stemmeler, K., Zellweger, C., Ridgeon, P., 2004. Two high-speed, portable GC systems designed for the measurement of non-methane hydrocarbons and PAN: results from the Jungfraujoch High Altitude Observatory. *J. Environ. Monit.* 6, 234.
- Williams, J., Roberts, J.M., Bertman, S.B., Stroud, C.A., Fehsenfeld, F.C., Baumann, K., Buhr, M.P., Knapp, K., Murphy, P.C., Nowick, M., Williams, E.J., 2000. A method for the airborne measurement of PAN, PPN, and MPAN. *J. Geophys. Res.* 105, 28943–28960.
- Xu, Z., Xue, L.K., Wang, T., Xia, T., Gao, Y., Louie, P.K.K., Luk, C.W.Y., 2015. Measurements of peroxyacetyl nitrate at a background site in the Pearl River Delta region: production efficiency and regional transport. *Aerosol Air Qual. Res.* 15, 833–841.
- Zellweger, C., Ammann, M., Buchmann, B., Hofer, P., Lugauer, M., Rüttimann, R., Streit, N., Weingartner, E., Baltensperger, U., 2000. Summertime NO_y speciation at the Jungfraujoch, 3580 m above sea level. *Switz. J. Geophys. Res.* 105, 6655–6667.
- Zellweger, C., Forrer, J., Hofer, P., Nyeki, S., Schwarzenbach, B., Weingartner, E., Ammann, M., Baltensperger, U., 2003. Partitioning of reactive nitrogen (NO_y) and dependence on meteorological conditions in the lower free troposphere. *Atmos. Chem. Phys.* 3, 779–796.
- Zhang, G., Mu, Y., Zhou, L., Zhang, C., Zhang, Y., Liu, J., Fang, S., Yao, B., 2015. Summertime distributions of peroxyacetyl nitrate (PAN) and peroxypropionyl nitrate (PPN) in Beijing: understanding the sources and major sink of PAN. *Atmos. Environ.* 103, 289–296.
- Zhang, J.M., Wang, T., Ding, A.J., Zhou, X.H., Xue, L.K., Poon, C.N., Wu, W.S., Gao, J., Zuo, H.C., Chen, J.M., Zhang, X.C., Fan, S.J., 2009. Continuous measurement of peroxyacetyl nitrate (PAN) in suburban and remote areas of western China. *Atmos. Environ.* 43, 228–237.
- Zhang, L., Jacob, D.J., Boersma, K.F., Jaffe, D.A., Olson, J.R., Bowman, K.W., Worden, J.R., Thompson, A.M., Avery, M.A., Cohen, R.C., Dibb, J.E., Flock, F.M., Fuelberg, H.E., Huey, L.G., McMillan, W.W., Singh, H.B., Weinheimer, A.J., 2008. Transpacific transport of ozone pollution and the effect of recent Asian emission increases on air quality in North America: an integrated analysis using satellite, aircraft, ozonesonde, and surface observations. *Atmos. Chem. Phys.* 8, 6117–6136.
- Zhang, L., Jaffe, D.A., 2017. Trends and sources of ozone and sub-micron aerosols at the Mt. Bachelor Observatory (MBO) during 2004–2015. *Atmos. Environ.* 165, 143–154.